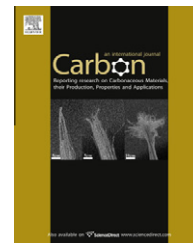


available at [www.sciencedirect.com](http://www.sciencedirect.com)journal homepage: [www.elsevier.com/locate/carbon](http://www.elsevier.com/locate/carbon)

## Letter to the Editor

# Tension–compression anisotropy of in-plane elastic modulus for pyrolytic carbon

Todd S. Gross <sup>a,\*</sup>, Khanh Nguyen <sup>a</sup>, Michael Buck <sup>b</sup>, Nikolay Timoshchuk <sup>a</sup>, Igor I. Tsukrov <sup>a</sup>, Boris Reznik <sup>c</sup>, Romana Piat <sup>b</sup>, Thomas Böhlke <sup>b</sup>

<sup>a</sup> Department of Mechanical Engineering, University of New Hampshire, Durham, NH 03824, USA

<sup>b</sup> Institute of Engineering Mechanics, Karlsruhe Institute of Technology (KIT), Karlsruhe, Germany

<sup>c</sup> Institute for Chemical Technology and Polymer Chemistry, Karlsruhe Institute of Technology (KIT), Karlsruhe, Germany

## ARTICLE INFO

## Article history:

Received 12 October 2010

Accepted 7 January 2011

Available online xxx

## ABSTRACT

We used standard strain gage methods to measure the anisotropic elastic constants for a sample of pyrolytic carbon. The in-plane elastic modulus exhibits significant tension–compression anisotropy –30.2 GPa in tension and 18.8 GPa in compression. The out-of-plane compressive modulus is 5.2 GPa and the Poisson's ratios are  $\nu_{12} = 0.35$  (compression),  $\nu_{23} = 0.16$  (tension), 0.22 (compression), and  $\nu_{21} = 0.97$  (tension). The tension–compression anisotropy is attributed to buckling, puckering, or bending of the graphene sheets in compression versus simple stretching in tension. The in-plane to out-of-plane anisotropy is expected from the microstructural anisotropy.

© 2011 Elsevier Ltd. All rights reserved.

This letter reports on measurements of the anisotropic elastic behavior of a sample of highly textured pyrolytic carbon produced by Schunk Kohlenstofftechnik GmbH, Heuchelheim, Germany. The structure has been characterized using optical microscopy, transmission electron microscopy, and ultrasound phase spectroscopy methods [1]. The strong microstructural anisotropy coupled with planar growth condition suggests that the elastic behavior should be transversely isotropic and this is supported by the ultrasound spectroscopy. We used standard strain gage methods to measure the in-plane and out-of-plane elastic modulus and all three Poisson's ratio values in both tension and compression on the same specimen as [1] and report our results in the following paragraphs.

The coordinate system is defined so that out-of-plane is the “1” direction and the in-plane directions are “2” and “3”. The schematic in Fig. 1 shows the orientation of the gages

for the in-plane measurements. The out-of-plane elastic modulus,  $E_1$ , and the out-of-plane Poisson's ratio,  $\nu_{13} = \nu_{12}$  were measured in uniaxial compression on nominally 2 mm by 6 mm sections of the material consisting of three layers glued together to avoid friction effects at the loading faces. We measured axial strain on the center section on opposing side of the specimen to ensure that the measurement was truly uniaxial and no significant bending was present. The transverse strain was measured by one gage and Poisson's ratio was always calculated from the gages on the same side of the specimen.

The in-plane modulus,  $E_2 (=E_3)$  and the Poisson's ratios ( $\nu_{21} = \nu_{31}$ ,  $\nu_{23} = \nu_{32}$ ) were measured in uniaxial compression and uniaxial tension. The tensile specimen was ~4 mm wide, approximately 20 mm long. The compression tests were performed on a 10 mm wide, 1.5 mm thick, and 5 mm high specimens. Again, gages measuring axial strain were affixed to

\* Corresponding author. Address: Department of Mechanical Engineering, University of New Hampshire, Kingsbury Hall W101, Durham, NH 03824-34591, USA.

E-mail address: [todd.gross@unh.edu](mailto:todd.gross@unh.edu) (T.S. Gross).

0008-6223/\$ - see front matter © 2011 Elsevier Ltd. All rights reserved.

doi:10.1016/j.carbon.2011.01.012

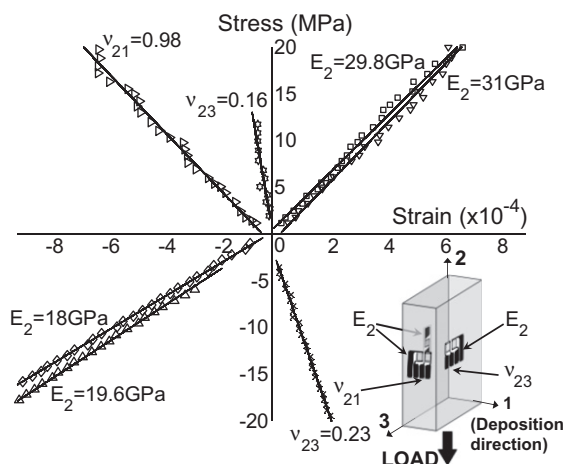


**Fig. 1 – Stress–strain curves for in-plane measurements in tension and in compression showing specimen orientation and location of strain gages for each elastic constant.**

both sides of the specimen to ensure uniaxial loading and a single gage was used to measure the transverse strain for Poisson's ratio. The Poisson's ratio ( $\nu_{21} = \nu_{31}$ ) was only measured in tension. All samples were obtained from the same disk and one sample was tested several times for each orientation. The specimens were loaded to stresses of 10–20 MPa and were referenced to the zero load state before and after loading. The load was measured with an 896 N (200 lb) load cell. The strain was inferred from the bridge imbalance with a strain resolution of  $\sim 10^{-6}$ . The uncertainty of the slope determination was approximately 0.1% based on the lumped uncertainties of the load, voltage, and dimension measurements. However, the uncertainty of the modulus measurement including variations in alignment is on the order of 1–2%. The modulus was determined from the average slope computed from the gages on the opposing faces of the specimen. The Poisson's ratio was calculated from the ratio of strains of the gages on the same face of the specimen and is therefore unaffected by the small bending moment. The elastic constants determined from linear regression of the load versus strain curves are summarized in Table 1.

The most significant finding is the observation of substantial tension–compression anisotropy of the in-plane elastic modulus;  $E_2 = 18.8$  GPa for compression and 30.2 GPa for tension and for the Poisson's ratio  $\nu_{23} = \nu_{32}$ . Fig. 1 shows the tension and compression stress–strain data for the in-plane measurements. This tension–compression anisotropy has

not been previously reported for pyrolytic carbon. However, Oya and Johnson [2] observed tension–compression anisotropy of the longitudinal elastic modulus and the yield strength in PAN-based fibers. They attributed the anisotropy to needle-like pores aligned along the length of the fiber.

The sample exhibits turbostratic structure in which the graphene planes are nominally parallel to the growth plane and are often kinked. This kinked character seems to be present at every level of microstructural scale. At the nanoscale, the microstructure consists of roughly aligned graphene planes that are kinked and have numerous planes that terminate in the middle of domain-like regions as seen in Fig. 2. Fractured specimens exhibit features where the layer thickness is on the order of micrometers as seen in the low magnification image in Fig. 3. Fig. 4 is a higher magnification image showing evidence of the kinked, turbostratic structure. On the microscale, the domains organize themselves into  $\sim 10$   $\mu\text{m}$  wide columnar features that exist through most of the thickness of the layer (see Fig. 1a in Ref. [1]).

One possible explanation for the tension–compression elastic anisotropy is that the graphene planes buckle or pucker in when loaded in compression in the plane of the graphene as suggested by Riter [3]. Another possibility is that kinks in the turbostratic structure deform by bending in compression but only straighten in tension. A third possibility is that there are disk-like voids between the coarse layers seen in the Fig. 3 and that they “buckle open” when loaded in compression.

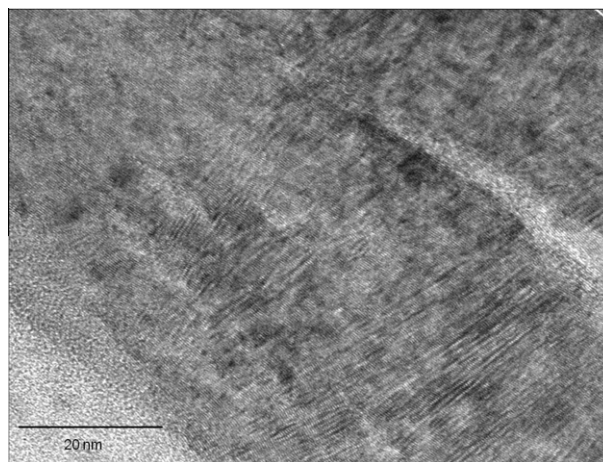


**Fig. 2 – TEM image at substrate interface showing kinked planes, small domains, and disordered regions between domains.**

**Table 1 – Comparison of elastic constants measured in this work to values obtained in three point bending [4] on similar material and by ultrasound phase spectroscopy [1] on the same material. The uncertainty values correspond to one standard deviation. The three point bending modulus range is for several different heat treatments and deposition conditions.**

	Tension	Compression	Three point bending [4]	Ultrasonic [1]
$E_1$ (GPa)	–	$5.2 \pm 0.3$	–	12.8
$E_2 = E_3$ (GPa)	$30.2 \pm 1.1$	$18.8 \pm 0.7$	6–16	27.1
$\nu_{12} = \nu_{13}$	–	$0.35 \pm 0.007$	–	0.22
$\nu_{23} = \nu_{32}$	$0.16 \pm 0.03$	$0.22 \pm 0.01$	–	0.35
$\nu_{21} = \nu_{31}$	$0.97 \pm .04$	–	–	0.47

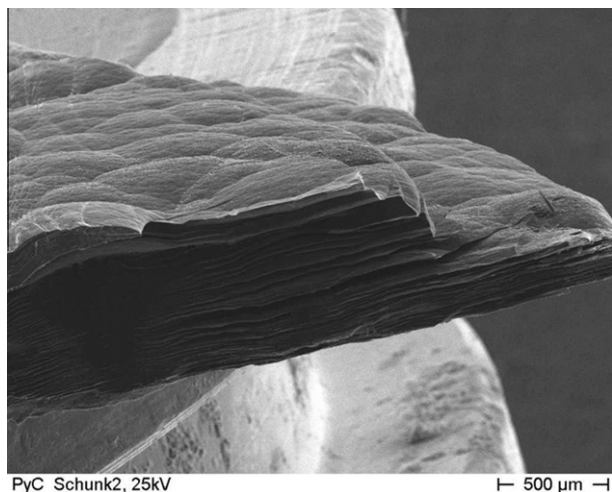


**Fig. 3 – SEM of fractured portion of the specimen showing layered structure.**

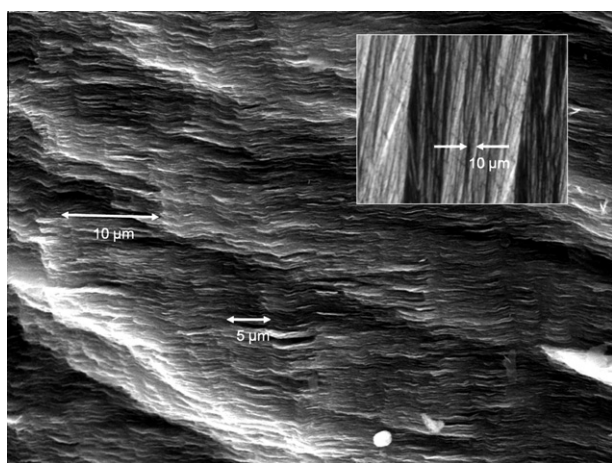


**Fig. 4 – SEM of fractured portion of the specimen showing turbostratic, kinked structure.**

There is also significant anisotropy ( $E_2/E_1 = 3.95$ ) between the in-plane and out-of-plane elastic modulus measured in compression (the out-of-plane elastic modulus in tension was not determined). Further, there is significant anisotropy in the Poisson's ratio in tension. The large observed value of  $\nu_{12} = \nu_{13} = 0.97$  is consistent with the degree of in-plane to out-of-plane anisotropy.

Guellali et al. [4] estimated the in-plane elastic modulus from three-point bending tests on similar material and report a range of reduced modulus values depending on heat treatment and deposition conditions. However, the equations they used to estimate the modulus are based on linear, isotropic elasticity as well as tension–compression isotropy. One could measure strain on both sides of a specimen in four-point

bending to detect tension–compression anisotropy using bend tests.

Gebert et al. [1] used ultrasound phase spectroscopy to measure all of the components of the stiffness matrix. We have converted their results to engineering modulus values for direct comparison in Table 1 but, given the large uncertainty on some of the stiffness matrix values, the comparison is only approximate. The in-plane modulus values are close to the values we measured in tension. The out-of-plane modulus is a factor of two lower than the ultrasound measurements. Like Guellali's work, the estimates they make are based on tension–compression isotropy. Since the correlation between acoustic velocity and elastic modulus is based on propagation of a longitudinal tension–compression wave, the apparent modulus inferred from ultrasound measurements will be an average of the tensile and compression modulus. The differences in Poisson's ratio measurements are probably correlated with the different degree of in-plane to out-of-plane anisotropy.

The lack of data for  $\nu_{12} = \nu_{13}$  for tensile loading and  $\nu_{21} = \nu_{31}$  in compression prevents us from evaluating whether the elastic constants satisfy the constraints on their values as dictated by symmetry and strain energy density arguments. Our future work will include measurements of all of the different components but we felt that the observation of tension–compression was an important finding.

## Acknowledgements

The authors gratefully acknowledge the financial support of the National Science Foundation (NSF) and German Science Foundation (DFG) through the Grant DMR-0806906 Materials World Network: Multi-Scale Study of Chemical Vapor Infiltrated Carbon/Carbon Composites. Romana Piat also acknowledges the support of DFG through the project PI 785/1-1 (Heisenberg fellowship).

## REFERENCES

- [1] Gebert J-M, Reznik B, Piat R, Viering B, Weidenmann K, Wanner A, et al. Elastic constants of high-texture pyrolytic carbon measured by ultrasound phase spectroscopy. *Carbon* 2010;48:3647–50.
- [2] Oya N, Johnson DJ. Longitudinal compressive behaviour and microstructure of PAN based carbon fibres. *Carbon* 2001;39:635–45.
- [3] Riter Jr JR. Interpretation of diamond and graphite compressibility data using molecular force constants. *J Chem Phys* 1970;52:5008–10.
- [4] Guellali M, Oberacker R, Hoffmann MJ. Influence of heat treatment on microstructure and properties of highly textured pyrocarbons deposited during CVD at about 1100 °C and above 2000 °C. *Compos Sci Technol* 2008;68(5):1122–30.